Supplementary Note S1

1.1 Introduction – Components of the contact force

The purpose of this note is to derive expressions used in the sea ice toolbox to calculate the components of the total contact force between interacting grains ($\mathbf{F}_{c,ij,n}$ and $\mathbf{F}_{c,ij,t}$ in the main text). In order to keep the notation concise and to limit the amount of indices used in the symbols, the index ij will not be used in the following text unless it is absolutely necessary. The amplitude of the two components can thus be written as:

$$F_{c,n} = k_n \delta_n - \gamma_n \frac{d\delta_n}{dt}, \tag{1}$$

$$F_{c,t} = k_t \delta_t - \gamma_t \frac{d\delta_t}{dt}, \tag{2}$$

where, by definition, $d\delta_n/dt$ and $d\delta_t/dt$ denote the normal and tangential component, respectively, of the relative velocity of the interacting particles. In a general case, the coefficients k_n, k_t, γ_n, γ_t are functions of the displacement (δ_n and δ_t), as well as the shape, size and material properties of interacting objects. Thus, the form of (1), (2) does not imply a linear relationship between, e.g., the normal repulsive force and the overlap δ_n. The exact form of k_n, k_t, γ_n, γ_t depends on the assumptions of a selected contact model and decides on the range of applicability of the DEM configuration based on that model (monodisperse or polydisperse systems, perfectly elastic or viscoelastic particles, fast collisions or semi-permanent contact, etc.). Among the models most frequently used in simulations of granular materials are the Hertzian [3] and linear spring/dashpot models for elastic particles, and the Kuwabara and Kono model for viscoelastic particles [5, 4, 2], which uses the Hertzian relation for the repulsive force (the first term on the right-hand side of equation 1) complemented with a dissipative term describing the viscoelastic energy loss. Apart from the works cited above, valuable details concerning (visco-)elastic contact models in a general context can be found, e.g., in [8, 9, 7, 10].
The models implemented in LIGGGHTS are described in the program documentation. They are formulated for spherical particles, typically used in granular models. Thus, in order to make the model suitable for sea ice simulations, analogous expressions for k_n, k_t, γ_n, γ_t had to be implemented, taking into account cylindrical geometry of the particles. In the following, the respective formulae – based on the Hertzian model – are derived and described; analogous formulae for spherical particles are provided for the sake of completeness and comparison. (It is worth noting that, apart from the force components discussed here, LIGGGHTS enables to add two other types of forces, namely cohesion and rolling friction; they are not taken into account in the sea ice toolbox and won't be discussed here.)

1.2 Definitions

Let us consider two objects, i and j, made of materials characterized by elastic moduli and Poisson ratios, E_i, ν_i and E_j, ν_j, respectively. In the following, we will consider two shapes of objects: spheres and disks. In both cases, r_i and r_j denote the radius of the objects. In the case of disks, additionally h_i and h_j denote their heights (thicknesses) and $h_m = \min\{h_i, h_j\}$.

Let us define the effective radius r_c and the effective mass m_c of the objects as:

$$r_c = \frac{r_i r_j}{r_i + r_j} \quad \text{and} \quad m_c = \frac{m_i m_j}{m_i + m_j}, \tag{3}$$

their effective contact modulus as:

$$E_c = \left(\frac{1 - \nu_i^2}{E_i} + \frac{1 - \nu_j^2}{E_j} \right)^{-1}, \tag{4}$$

and their shear modulus as:

$$G_c = \frac{1}{2} \left(\frac{(2 + \nu_i)(1 - \nu_i)}{E_i} + \frac{(2 + \nu_j)(1 - \nu_j)}{E_j} \right)^{-1}. \tag{5}$$

For objects made of identical materials ($E_i = E_j = E$, $\nu_i = \nu_j = \nu$):

$$E_c = \frac{E}{2(1 - \nu^2)} \quad \text{and} \quad G_c = \frac{E}{4(2 + \nu)(1 - \nu)}. \tag{6}$$

The normal overlap (displacement) δ_n between the spheres/disks is measured along the line connecting their centers and is defined as:

$$\delta_n = r_i + r_j - |\mathbf{x}_i - \mathbf{x}_j|, \tag{7}$$

where $\mathbf{x}_i$ and $\mathbf{x}_j$ denote the positions of the centers. For objects in contact with each other, $\delta_n \geq 0$. The tangential displacement δ_t is measured in the direction perpendicular to that of δ_n, i.e., within the plane of contact. It accounts for the "history" effects of the contact.
The essential difference between spherical and cylindrical objects in contact is the shape of the contact surface. In the case of spheres, the contact area is circular, with a radius increasing with increasing normal force; in the case of disks it is rectangular, with a constant height equal to h_m and width increasing with increasing normal force.
If one of the two objects (let's say, j) is a wall, the equations derived further remain valid under an assumption that r_j denotes the local radius of curvature of the wall. For a flat wall, $r_j \to \infty$ (i.e., $r_c = r_i$ and $m_c = m_i$), δ_n is calculated based on the normal distance of the object's center from the wall, and δ_t is calculated as a displacement of the object's center in a direction parallel to the wall.
Finally, a number of contact models make use of a relationship between the damping ratio β and the restitution coefficient e_r. For underdamped systems:

$$\beta = \frac{\ln e_r}{\left(\ln^2 e_r + \pi^2 \right)^{1/2}}. \tag{8}$$

1.3 The Hertz contact mechanics

1.3.1 Two elastic spheres

Under the assumptions of the Hertz contact theory [3, 1, 10], under a normal force of the magnitude $F_{c,n}$, the radius r_0 of the contact circle between two elastic spheres is given by:

$$r_0 = \left(\frac{3 r_c F_{c,n}}{4 E_c} \right)^{1/3}, \tag{9}$$

and the normal displacement δ_n is given by:

$$\delta_n = \frac{r_0^2}{r_c}. \tag{10}$$

From (9) and (10), the force between two overlapping spheres equals:

$$F_{c,n} = \frac{4}{3} E_c \delta_n^{3/2} r_c^{1/2}. \tag{11}$$

Thus, k_n in (1) is given as:

$$k_n = \frac{4}{3} E_c (\delta_n r_c)^{1/2}. \tag{12}$$

1.3.2 Two elastic cylinders

In this case, the normal displacement is given by [6] (see also [7] for the case of identical disks):

$$\delta_n = \frac{F_{c,n}}{\pi h_m E_c} \left[1 + \ln \frac{2\pi h_m^3 E_c}{r_c F_{c,n}} \right]. \tag{13}$$

In DEM, $F_{c,n}(\delta_n)$ has to be calculated rather than $\delta_n(F_{c,n})$. Unfortunately, whereas in the case of spheres the exact form of $F_{c,n}(\delta_n)$ can be found easily – as given by (11) – expression (13) cannot be inverted analytically and therefore an approximate solution has to be found. To this end, we introduce the following non-dimensional variables:

$$\delta_n^* = \frac{\delta_n r_c}{2h_m^2} \quad \text{and} \quad F_{c,n}^* = \frac{r_c F_{c,n}}{2\pi E_c h_m^3}, \tag{14}$$

so that (13) can be written as:

$$\delta_n^* = F_{c,n}^* (1 - \ln F_{c,n}^*). \tag{15}$$

In the present context, this equation is valid for $F_{c,n}^* \ll 1$, so that $F_{c,n}^*$ is an increasing function of δ_n^*, i.e., the overlap increases with the applied force. We search for an approximate solution in the form:

$$\tilde{F}^*(\delta_n^*) = \delta_n^* f(\delta_n^*), \tag{16}$$

where f denotes a function obtained by a least-square fit of a prescribed functional form (see below) to numerically calculated set of pairs of values $(\delta_n^*, F_{c,n}^*/\delta_n^*)$. After returning to a dimensional form, we obtain an approximate expression for the normal contact force between two disks, $F_{c,n}$:

$$F_{c,n} = \pi E_c h_m \delta_n f\left(\frac{\delta_n r_c}{2h_m^2} \right), \tag{17}$$

so that k_n in (1) is given by:

$$k_n = \pi E_c h_m f\left(\frac{\delta_n r_c}{2h_m^2} \right), \tag{18}$$

Generally, $f(x)$ is a decreasing function, i.e., its values are larger for larger disk height h_m and smaller relative radius r_c and normal displacement δ_n. In the sea ice toolbox, a rational expression is used for f:

$$f(x) = \frac{p_1 x^2 + p_2 x + p_3}{x^2 + q_1 x + q_2}. \tag{19}$$

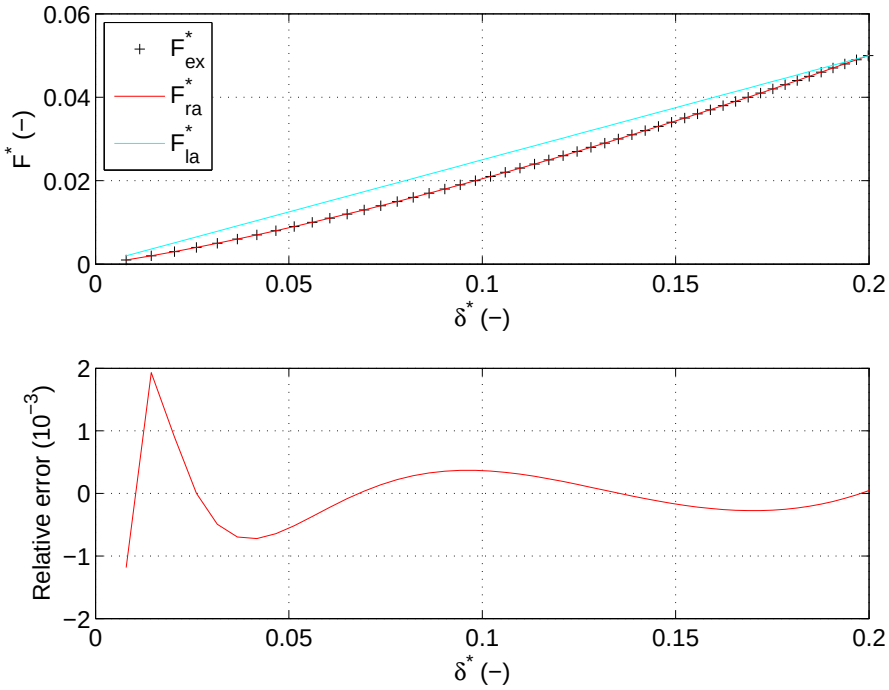

Supplementary Figure 1: Exact (black crosses) and least-square-fit (red curve: rational fit, blue curve: linear fit) solutions $F^*_{c,n}(\delta^*)$ of equation (15). The lower plot shows the relative error of the rational fit.

The coefficients obtained for $x \in [0, 0.2]$ are: $p_1 = 0.9117$, $p_2 = 0.2722$, $p_3 = 0.003324$, $q_1 = 1.524$, and $q_2 = 0.03159$. Figure 1 shows the approximate solution (red curve) and its relative error – both in nondimensional form. Figure 2a–c illustrates how this approximation performs for a number of (r_c, h_m) combinations. The contact force between spheres with the same r_c is shown for reference. Not surprisingly, for a given overlap δ_n, the difference between the contact force for spheres and disks increases with increasing disk height – this difference is a measure of the error that is made when the original LIGGGHTS model, suitable for spherical geometry, is used for disk-shaped particles. Also, as can be seen in Fig. 2a–c, the error of the approximate model (20),(19) remains small for a wide range of r_c and h_m values, which is particularly important in view of the very strong polydispersity of sea ice. Noticeable overestimation is present only for very small r_c and large h_m (blue curve in Fig. 2a); noticeable underestimation – for large r_c and small h_m (green curve in Fig. 2c). Generally, equation (3) implies that $0 < r_c \leq \frac{1}{2}\max\{r_i, r_j\}$, with small r_c in situations when at least one of the disks is very small, and with large r_c in situations when both disks are large. Hence, the contact force will tend to be slightly overestimated for thick and small disks and underestimated for thin and large disks.

Finally, it is worth noting that instead of (13), a simple linear expression for $F_{c,n}(\delta_n)$ is sometimes used in DEMs in the form:

$$F_{c,n} = \frac{\pi}{4} h_m E_c \delta_n, \tag{20}$$

in which the repulsive force does not depend on r_c. For the sake of comparison, this solution is shown in Figs. 1 (blue curve) and 2d for the same set of h_m as in Fig. 2a–c.

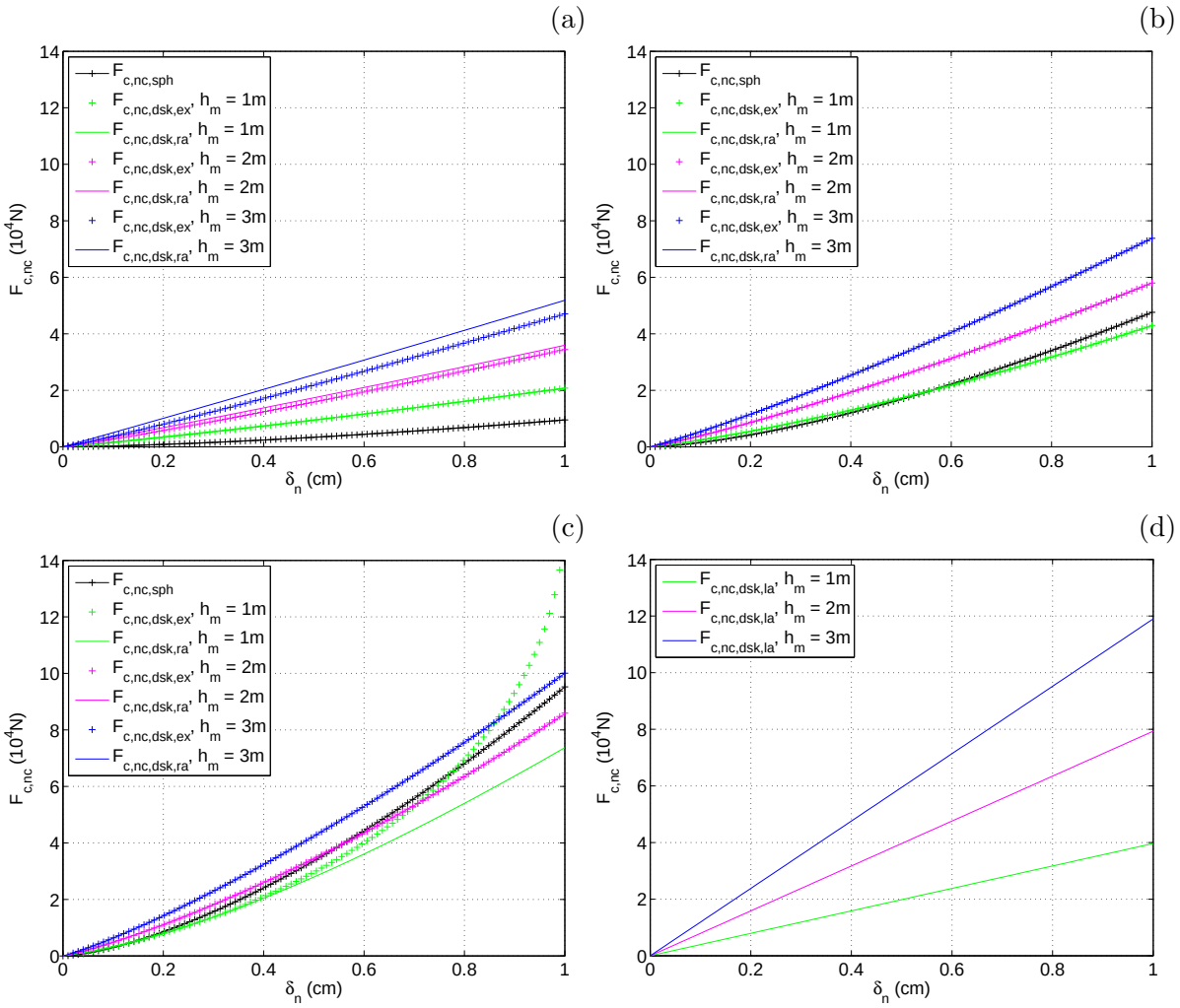

Supplementary Figure 2: Normal contact force $F_{c,n}$ between pairs of spheres (black) and disks with various height h_m (color). In panels (a–c), values obtained with the exact formula (13) are shown with crosses, and values obtained with the rational approximation (20),(19) are shown with continuous curves, for $r_c = 2$ m (a), $r_c = 50$ m (b), and $r_c = 200$ m (c). Panel (d) shows values obtained with the linear approximation (20), which does not depend on r_c. Calculations performed for $E_c = 5.05 \cdot 10^6$ Pa.

1.4 The viscoelastic models in LIGGGHTS

As already mentioned, in a number of viscoelastic contact models the Hertzian theory is used to calculate the normal repulsive force (i.e., the k_n coefficient), as well as to estimate the shear and damping terms in (1) and (2). In LIGGGHTS, two versions of the linear (Hookean) model and two versions of the Kuwabara and Kono (Hertzian) model are available, each for objects with spherical geometry. In a simple version of the Hertzian model, the coefficients in (1),(2) are calculated based on user-specified constants $\bar{k}_n$, $\bar{k}_t$, $\bar{\gamma}_n$, $\bar{\gamma}_t$ representing the analyzed material:

$$k_n = \sqrt{r_c \delta_n} \bar{k}_n, \tag{21}$$

$$k_t = \sqrt{r_c \delta_n} \bar{k}_t, \tag{22}$$

$$\gamma_n = \sqrt{r_c \delta_n} m_c \bar{\gamma}_n, \tag{23}$$

$$\gamma_t = \sqrt{r_c \delta_n} m_c \bar{\gamma}_t. \tag{24}$$

In its full version, k_n is calculated from (12) and the remaining coefficients are given by:

$$k_t = 6\frac{G_c}{E_c} k_n, \tag{25}$$

$$\gamma_n = -\beta\sqrt{5 k_n m_c}, \tag{26}$$

$$\gamma_t = -2\beta\sqrt{5\frac{G_c}{E_c} k_n m_c}. \tag{27}$$

Exactly this model is used in the sea ice toolbox, with the only difference being that k_n is calculated from (18),(19).

References

[1] G.G. Adams and M. Nosonovsky. Contact modeling – forces. *Tribology Intern.*, 33:431–442, 2000.

[2] N.V. Brilliantov, F. Spahn, J.-M. Hertzsch, and T. Pöschel. Model for collisions in granular gases. *Phys. Rev. E*, 53:5382–5392, 1996.

[3] H. Hertz. Ueber die Berührung fester elastischer Körper. *J. reine angewandte Mathematik*, 92:156–171, 1881.

[4] J.-M. Hertzsch, F. Spahn, and N.V. Brilliantov. On low-velocity collisions of viscoelastic particles. *J. Phys. II France*, 5:1725–1738, 1995.

[5] G. Kuwabara and K. Kono. Restitution coefficient in a collision between two spheres. *Jpn. J. Appl. Phys.*, 26:1230–1233, 1987.

[6] M.J. Puttock and E.G. Thwaite. Elastic compression of spheres and cylinders at point and line contact. Technical Report No. 25, Australian Commonwealth Scientific and Industrial Research Organization, 1969. 64 pp.

[7] T. Schwager. Coefficient of restitution for viscoelastic disks. *Phys. Rev. E*, 75:051305, 2007.

[8] A.B. Stevens and C.M. Hrenya. Comparison of soft-sphere models to measurements of collision properties during normal impacts. *Powder Tech.*, 154:99–109, 2005.

[9] H.P. Zhang and H.A. Makse. Jamming transition in emulsions and granular materials. *Phys. Rev. E*, 72:011301, 2005.

[10] Y. Zhou. A theoretical model of collision between soft-spheres with Hertz elastic loading and nonlinear plastic unloading. *Theor. Appl. Mech. Lett.*, 1:041006, 2011.

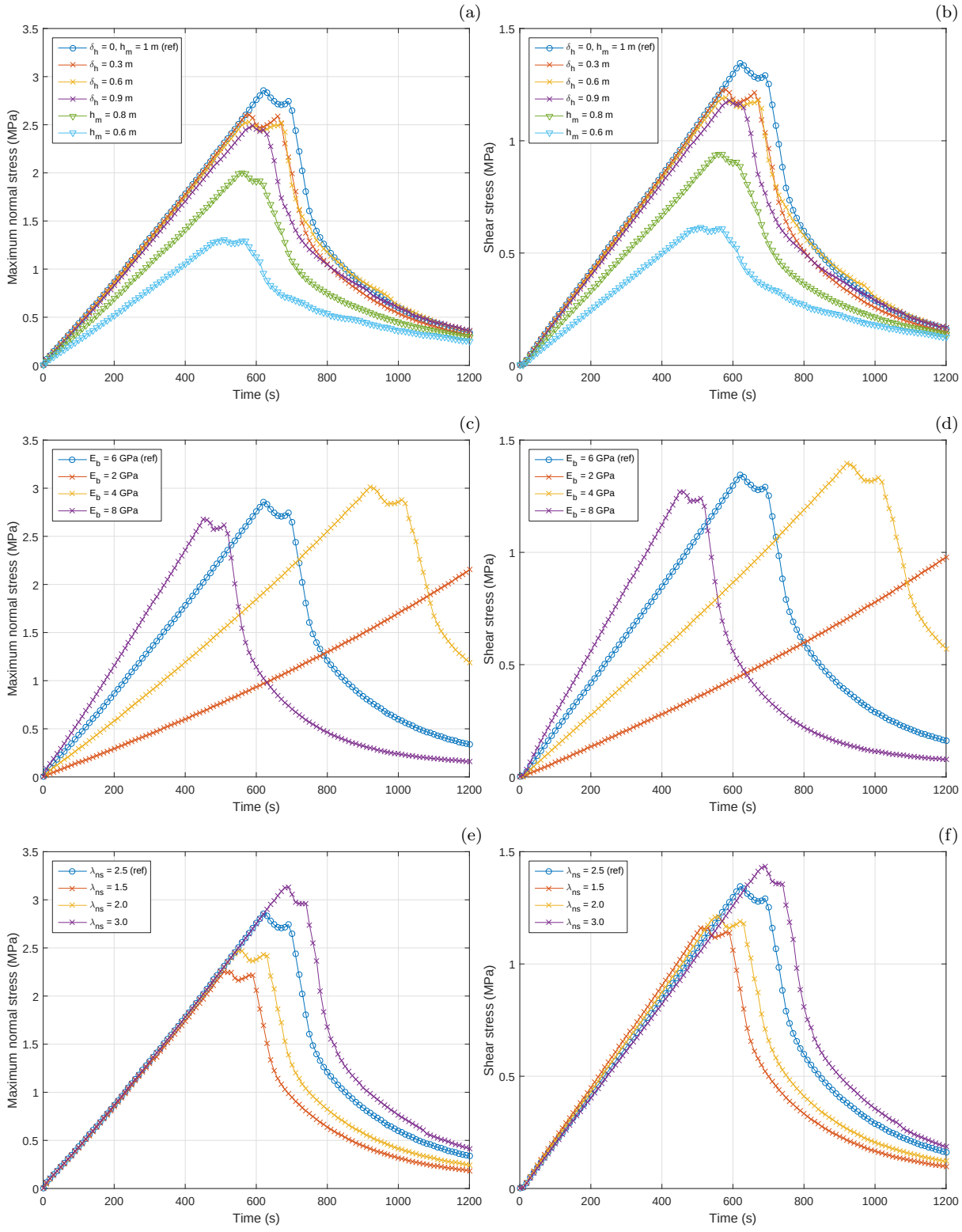

Supplementary Figure 3: Amplitude of the maximum normal (a,c,e) and shear (b,d,f) stress due to bonded interactions in simulations under uniaxial tensile strain, with variable model parameters.

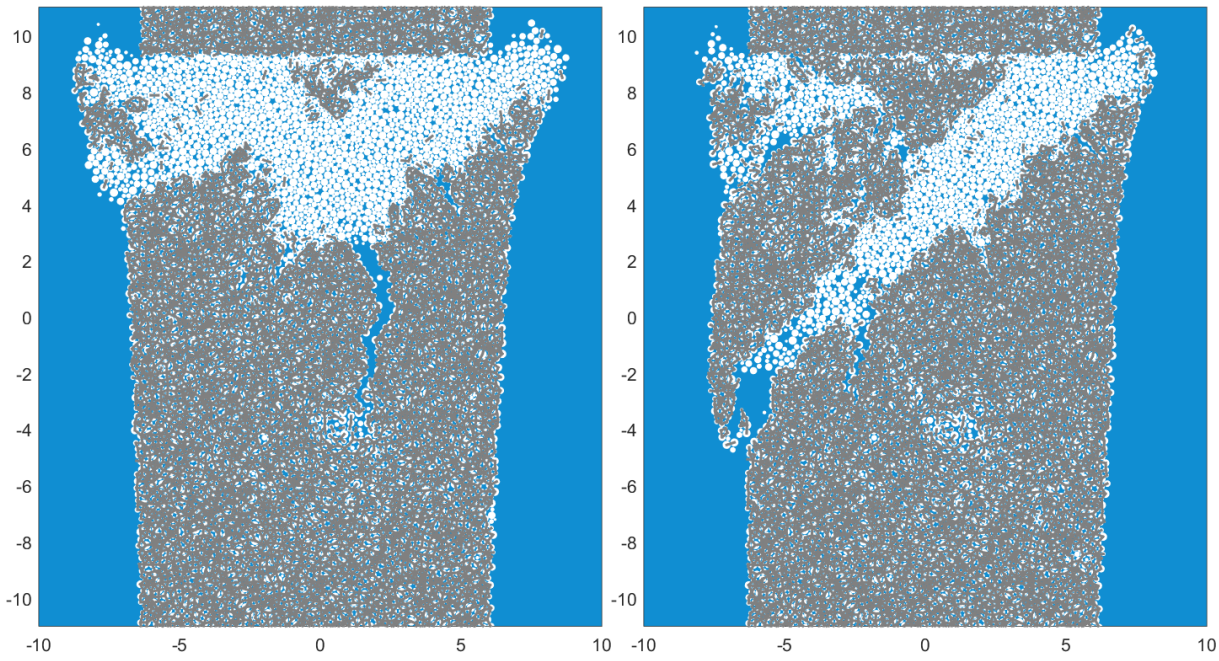

Supplementary Figure 4: Example damage patterns obtained in simulations of an initially compact sample under uniaxial compressive strain with $\varepsilon_0 = 0.5 \cdot 10^{-4}$ s^{-1} (left) and $\varepsilon_0 = 0.35 \cdot 10^{-4}$ s^{-1} (right). Thick gray lines show the bonds between grains. Model parameters as in the reference run except $\varepsilon = 0.40 \cdot 10^{-4}$ s^{-1} (a) and $\varepsilon = 0.35 \cdot 10^{-4}$ s^{-1} (b).

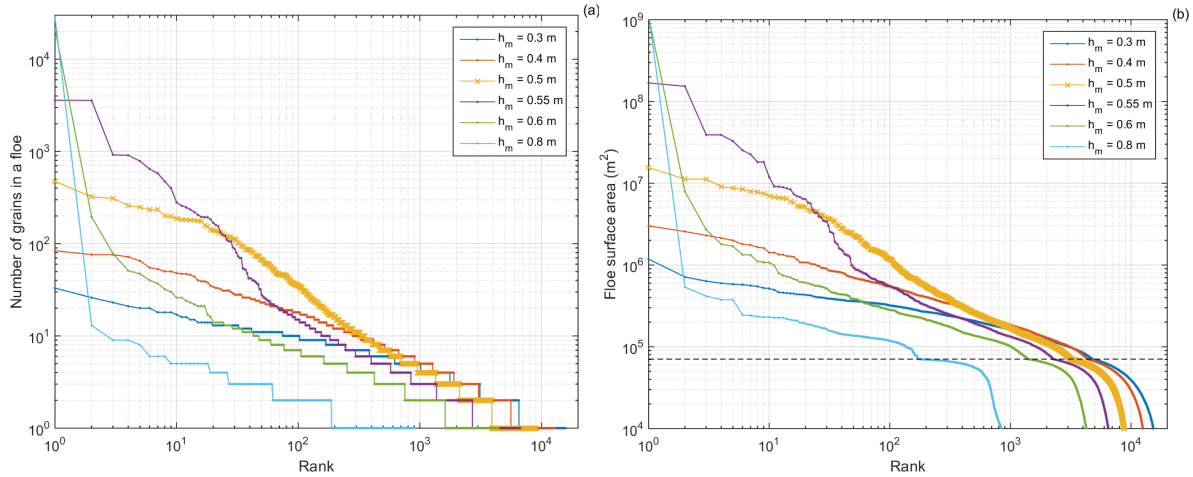

Supplementary Figure 5: Rank-order statistics of floe sizes (a: number of grains in a floe; b: floe surface area) obtained in simulations with different mean bond thickness h_m. The dashed line in (b) marks the area of the largest individual grain in the ensemble. Results of the reference run are shown with crosses.

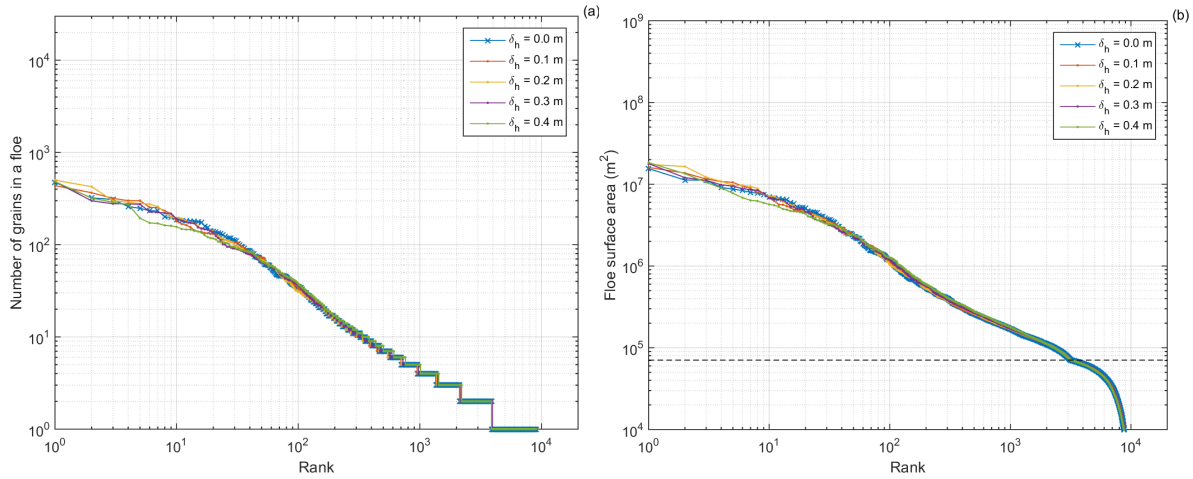

Supplementary Figure 6: As in Fig. 5, but for simulations with different width of bond-thickness distribution δ_h.

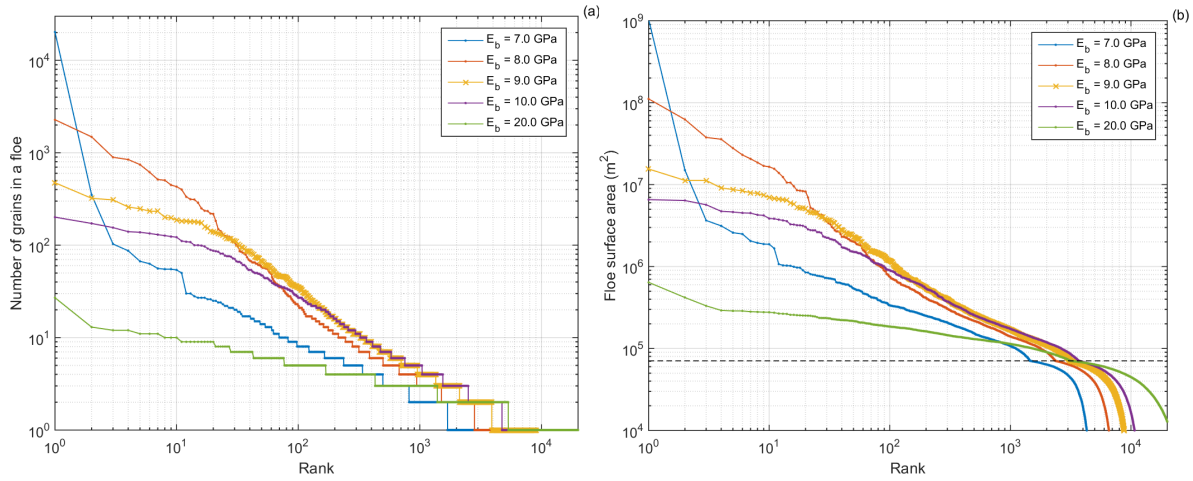

Supplementary Figure 7: As in Fig. 5, but for simulations with different bond elastic modulus E_b.